Research Square

Preprints are preliminary reports that have not undergone peer review.
They should not be considered conclusive, used to inform clinical practice,
or referenced by the media as validated information.

Number Statistics and State-Dependent Charging in aDriven Optomechanical Quantum Battery

Syed Jamal Anwar

sjamalanwar@gmail.com

Quaid-i-Azam University

S. Abdul Khalek S. Abdul Khalek

Taif University

Research Article

Keywords:

Posted Date: November 17th, 2026

DOI: https://doi.org/10.21203/rs.3.rs-11356085/v1

License: This work is licensed under a Creative Commons Attribution 4.0 International License.
Read Full License

Additional Declarations: No competing interests reported.

Number Statistics and State-Dependent Charging in a Driven Optomechanical Quantum Battery

S. Jamal Anwar [1,*], S. Abdel-Khalek [2]

[1]Department of Physics, Quaid-i-Azam University, Islamabad 45320, Pakistan
[2]Department of Physics, Faculty of Science, Sohag University, Sohag 82524, Egypt

October 4, 2026

Abstract

We investigate how the initial quantum state of a mechanical mode affects the charging of a two-cell atomic quantum battery embedded in a driven optomechanical cavity. To separate state structure from the trivial effect of initial mean energy, we compare Fock, coherent, thermal, squeezed-vacuum and even-cat mechanical states with the same mean occupation, $\langle n_b \rangle = 1$, and optimize the cavity detuning separately for each state. The dynamics are obtained from the full rotating-frame Hamiltonian within a finite Fock-space truncation rather than from the second-order effective model used in earlier work. At the optimized detunings the maximum normalized local ergotropy is approximately 0.280 for the Fock state, 0.094 for the coherent state, 0.033 for the squeezed vacuum, 0.032 for the even cat and 0.022 for the thermal state. Thus equal initial mechanical mean energy does not imply equal charging performance. This comparison should not be interpreted as matching the *total* energy supplied during the protocol, because the continuously applied classical drive can perform a state-dependent amount of work.

Wigner negativity does not order the charging performance. In particular, coherent, thermal and ideal squeezed-vacuum states all have non-negative Wigner functions, while the Wigner-negative even cat still underperforms the coherent state. Number statistics provide a more useful, though not complete, diagnostic: the two best chargers have the smallest number variance, whereas variance and the Mandel parameter do not strictly order the three broader states. A scan of the quadratic optomechanical coupling is consistent with a number-dependent detuning mechanism: the Fock-to-coherent ergotropy ratio rises from about 1.33 at $G_2 = 0$ to 5.17 at $G_2 = 0.08\,\omega_m$. The residual advantage at $G_2 = 0$ shows that the quadratic term amplifies, rather than solely creates, the state dependence. Reduced-truncation Lindblad calculations suggest that the qualitative ordering is robust to modest cavity and mechanical losses for the chosen parameters, while a thermal mechanical bath strongly degrades the Fock-state advantage. The results identify charger number statistics and state-dependent resonance structure as useful design variables, but the strong single-photon nonlinear coupling assumed here and the untracked work supplied by the drive should be kept in mind when assessing experimental feasibility.

Keywords: quantum battery; ergotropy; cavity optomechanics; mechanical quantum states; number statistics; Mandel parameter; Wigner function; quadratic optomechanical coupling; quantum thermodynamics.

1 Introduction

Quantum thermodynamics asks what happens to familiar ideas such as work, heat and efficiency when the working substance is small enough that quantum mechanics cannot be ignored [1–3].

*Corresponding author: sjamalanwar@gmail.com

One of the most concrete questions in that programme is deceptively simple: if we store energy in a quantum system, how much of it can we actually get back out? In general, only the part that can be removed by a cyclic unitary operation is useful, and that quantity has a name – the ergotropy – introduced in a form we still use today by Allahverdyan, Balian and Nieuwenhuizen [4], building on older results about passive states due to Pusz and Woronowicz [5] and Lenard [6]. A system engineered to store energy and later release it in this way has come to be called a *quantum battery* [7–10].

The field grew quickly once it became clear that quantum batteries might charge in ways that classical ones cannot. Alicki and Fannes showed that entangling operations across many copies can boost the extractable work [7]; Binder and co-workers pointed out that collective charging can be genuinely faster [8]; and Campaioli *et al.* put bounds on how much of a speed-up is possible at all [12]. Ferraro and colleagues then showed that a Dicke-type battery, in which many two-level systems share a single cavity mode, can charge with a power that grows faster than the number of cells [13]. Since then a good deal of effort has gone into understanding where such advantages really come from. Andolina and co-workers argued that correlations, which look like the obvious resource, in fact become irrelevant in the many-body limit – a result they called asymptotic freedom [14, 15]. Rossini *et al.* found genuine quantum speed-ups in Sachdev–Ye–Kitaev batteries [16], while Gyhm, Šafránek and Rosa proved that an extensive charging advantage is impossible without global operations [17]. Julià-Farré and colleagues derived general bounds on both capacity and power [18].

Alongside these general results, a long list of concrete platforms has been proposed. Spin chains were among the first [19, 20], including many-body localised [21] and deliberately disordered variants [22–24]. Atoms in optical cavities remain the workhorse [14, 25–27], and superconducting circuits have produced some of the most convincing hardware [28–30]. Organic microcavities gave one of the first experimental demonstrations of superabsorption in a battery-like setting [31], and NMR star-topology spin systems have been used to investigate charging in the laboratory [32]. Related experiments on single-atom heat engines [33], trapped-ion refrigerators [34, 35] and microscopic engines exploiting genuine quantum effects [36] have shown that the wider field of quantum thermal devices has moved firmly into the experimental era.

The obstacle that will not go away is decoherence. A battery that leaks its charge is not much use, and self-discharging has been studied from several angles: through disorder [24, 37], through charge-switchable designs [38], through dark states that hide the stored energy from the environment [39, 40], and through non-Markovian reservoir engineering [41, 42]. Running through much of this work is a question that has never been settled cleanly: what role, if any, do quantum correlations play in charging? Several groups have looked specifically at entanglement and coherence during the charging process [43–45], and the honest summary is that no universal relationship has been established.

Cavity optomechanics is an attractive setting in which to ask these questions [46–48]. A light field and a mechanical oscillator are coupled by radiation pressure, which brings quantum behaviour into objects large enough to see, and gives the experimenter an unusual number of knobs to turn [49, 50]. Optomechanical devices have become outstanding sensors [51–53], including for very weak gravitational signals [54–56], and they serve as transducers between microwave and optical domains [57, 58] and as elements in quantum information processing [59, 60]. Adding atoms to the cavity produces a hybrid system that is more complicated but also far more controllable [61–64].

Two developments make optomechanics particularly relevant here. The first is that mechanical resonators can now be prepared in genuinely non-classical states. Ground-state or near-ground-state control has been achieved in electromechanical [65], optomechanical [66], piezoelectric [67], levitated [68, 69], and measurement-based nanomechanical platforms [70]. Single-phonon Fock states have been created and verified [71, 72], multi-phonon Fock states have been assembled in bulk acoustic resonators [73], surface acoustic wave phonons have been controlled one at a

time [74, 75], mechanical squeezing has been demonstrated [76–78], motion has been entangled with microwave fields [79, 80], and – most strikingly – Schrödinger cat states of a 16-microgram oscillator have been reported [81]. In other words, the exotic charger states we compare in this paper are no longer purely theoretical.

The second development is the quadratic, or membrane-in-the-middle, coupling. When the mechanical element sits at a node or antinode of the cavity field the linear coupling vanishes and the leading interaction goes as the square of the displacement [82–84]. This changes the physics qualitatively, because the cavity frequency now shifts with phonon *number* rather than position [85, 86]. It has been proposed as a route to phonon-number-resolved measurements and to macroscopic superposition-state engineering [87, 88]. This number sensitivity motivates the mechanism tested below, although the full dynamics also contain linear-coupling and two-phonon contributions.

The comparison of charger states requires some care with terminology. A negative Wigner function is a useful witness of non-Gaussian quantum structure, but it is not a universal test of non-classicality: an ideal squeezed vacuum is non-classical while its Wigner function remains Gaussian and non-negative [93, 100]. Conversely, the Mandel parameter probes number statistics. A negative value, $Q < 0$, is a sufficient witness of sub-Poissonian statistics [99], whereas $Q \geq 0$ does not imply a classical state. These diagnostics therefore answer different physical questions and should not be used interchangeably. Phase-space negativity has important operational roles in several continuous-variable resource theories [91, 92, 94], while alternative notions of optical non-classicality include the Glauber–Sudarshan P representation [89, 90], nonclassical distance [95], observable P-function criteria [96, 97], and entanglement potential [98].

Our study is motivated directly by the recent optomechanical quantum-battery model of Shokri, Faizi and Arjmandi [11], which reported a strong correspondence between charging indicators, entanglement and Mandel parameters for restricted initial charger states. In a single-excitation manifold one must be especially cautious: if a mode is restricted to $n \in \{0, 1\}$, then $\langle n^2 \rangle = \langle n \rangle$ and

$$Q = \frac{\langle n^2 \rangle - \langle n \rangle^2}{\langle n \rangle} - 1 = -\langle n \rangle. \tag{1}$$

In that case a correlation between Q and a quantity that also grows with excitation number can be partly kinematic rather than evidence that Q itself is the operative resource.

We therefore compare substantially different mechanical states while fixing their initial mean occupation. The comparison is deliberately stricter in a second respect: the cavity detuning is optimized separately for each state for the headline results, so a broad state is not penalized merely because a shared operating point happens to favor another state. These controls isolate the influence of state structure from the initial mean mechanical energy, although they do not equalize the total work supplied by the continuous classical drive. Our numerical results show that a number-definite Fock state and a coherent state are the two best performers at the chosen operating point; Wigner negativity does not reproduce the ranking; and increasing the quadratic optomechanical coupling strongly magnifies the difference between narrow and broad number distributions. The association with number variance is useful but not exact, so we treat it as a mechanism-guided diagnostic rather than a universal resource law.

2 Model and derivation

We consider two identical two-level atoms, with transition frequency ω_0, placed inside a single-mode optical cavity of frequency ω_f. One cavity mirror is free to vibrate as a mechanical oscillator of frequency ω_m and effective mass m, and the cavity is driven by an external laser of frequency ω_l and amplitude E_l. The two atoms constitute the quantum battery; the optical and mechanical modes together are the charger. This is the standard hybrid atom–optomechanical arrangement

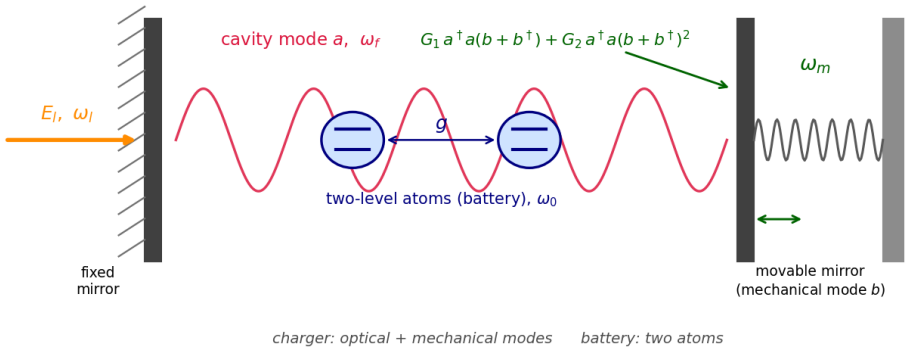


Figure 1: Sketch of the system. Two two-level atoms of transition frequency ω_0 (the battery) sit inside an optical cavity of frequency ω_f formed by a fixed mirror and a movable one. The movable mirror is a mechanical oscillator of frequency ω_m (mode b) and couples to the intracavity intensity both linearly (G_1) and quadratically (G_2); the latter is the membrane-in-the-middle coupling that will prove essential. The atoms exchange excitations with the cavity mode at rate g, and the cavity is driven by an external laser of amplitude E_l and frequency ω_l. The optical and mechanical modes together act as the charger; the mechanical mode carries the energy whose statistics we vary.

[46, 61, 63]. Setting $\hbar = 1$, the Hamiltonian is

$$H = H_{\text{free}} + H_{\text{int}}, \tag{2}$$

with the free part

$$H_{\text{free}} = \underbrace{\sum_{i=1,2} \frac{\omega_0}{2}\sigma_z^i}_{H_B} + \underbrace{\omega_f a^\dagger a + \omega_m b^\dagger b}_{H_C}, \tag{3}$$

and the interaction part

$$H_{\text{int}} = g\sum_{i=1,2}\left(a\sigma_+^i + a^\dagger\sigma_-^i\right) + G_1 a^\dagger a\,(b+b^\dagger) + G_2 a^\dagger a\,(b+b^\dagger)^2 + E_l\left(ae^{i\omega_l t} + a^\dagger e^{-i\omega_l t}\right). \tag{4}$$

Here a and b annihilate a cavity photon and a mechanical phonon, respectively, $\sigma_+ = |e\rangle\langle g|$ and $\sigma_- = |g\rangle\langle e|$ are the atomic ladder operators, and g is the atom–field coupling. Writing the mechanical displacement as $x = x_{\text{zpf}}(b + b^\dagger)$, with $x_{\text{zpf}} = (2m\omega_m)^{-1/2}$ for $\hbar = 1$, the local expansion of the cavity frequency gives

$$G_1 = x_{\text{zpf}}\left.\frac{\partial\omega_f}{\partial x}\right|_0, \qquad G_2 = \frac{x_{\text{zpf}}^2}{2}\left.\frac{\partial^2\omega_f}{\partial x^2}\right|_0. \tag{5}$$

The signs and relative magnitudes of G_1 and G_2 are geometry dependent. Quadratic coupling can be enhanced in membrane-in-the-middle and related multimode geometries [82–84]; operating away from an exact symmetry point, or using a more general nonlinear geometry, can leave both linear and quadratic terms present. Quadratic optomechanics has been analysed theoretically in Refs. [85, 88] and observed in the stationary regime in Ref. [86]. The final term in Eq. (4) is the classical cavity drive.

Removing the explicit time dependence. The drive makes Eq. (2) time dependent, which is inconvenient. We therefore move to the frame rotating at the laser frequency, generated by

$$R(t) = \exp\Big[-i\omega_l t\Big(a^\dagger a + \sum_i \tfrac{1}{2}\sigma_z^i\Big)\Big]. \tag{6}$$

Under $H \to R^\dagger H R - i R^\dagger \dot{R}$ the operators transform as $a \to a e^{-i\omega_l t}$ and $\sigma_- \to \sigma_- e^{-i\omega_l t}$. The Jaynes–Cummings term is invariant, because the two exponentials cancel:

$$a\sigma_+ e^{-i\omega_l t} e^{+i\omega_l t} = a\sigma_+. \tag{7}$$

The drive becomes static for the same reason, and the optomechanical terms are untouched since they contain $a^\dagger a$. What changes are the free energies, which turn into detunings. The result is a fully time-independent Hamiltonian,

$$\boxed{\begin{aligned} H = \Delta_c a^\dagger a + \frac{\Delta_a}{2} \sum_{i=1,2} \sigma_z^i + \omega_m b^\dagger b + g \sum_{i=1,2} \left(a\sigma_+^i + a^\dagger \sigma_-^i \right) \\ + G_1 a^\dagger a (b + b^\dagger) + G_2 a^\dagger a (b + b^\dagger)^2 + E_l (a + a^\dagger) \end{aligned}} \tag{8}$$

where

$$\Delta_c = \omega_f - \omega_l, \qquad \Delta_a = \omega_0 - \omega_l. \tag{9}$$

Two features of Eq. (8) deserve emphasis. First, the optical frequencies enter through detunings, which is the natural description of a driven cavity. Second, we propagate Eq. (8) directly rather than placing the near-resonant drive inside a second-order off-resonant coarse-graining. The James–Jerke construction [102, 103] is useful when eliminated harmonics are fast compared with the dynamics of interest, but a resonant or near-resonant static term must be retained explicitly. Our numerical results therefore refer to the full rotating-frame Hamiltonian within the stated Fock-space truncation, not to the effective Hamiltonian of the earlier single-excitation treatment [11].

Reference detuning and state-dependent resonance. The quadratic interaction makes different phonon-number sectors experience different optical shifts. Indeed,

$$(b + b^\dagger)^2 = 2b^\dagger b + 1 + b^2 + b^{\dagger 2}, \tag{10}$$

so its number-conserving part contains $G_2 a^\dagger a (2n_b + 1)$. The linear coupling also produces a photon-number-dependent polaron correction of order G_1^2/ω_m. Consequently there is no unique bare-cavity detuning that is simultaneously optimal for every component of a broad mechanical number distribution.

For broad parameter scans we use the same reproducible reference prescription as in the supplied numerical data,

$$\boxed{\Delta_c^{\mathrm{ref}} = -\left[G_2 \left(2n_{\mathrm{ref}} + 1 \right) + \frac{G_1^2}{\omega_m} \right],} \tag{11}$$

with $n_{\mathrm{ref}} = \langle n_b \rangle$. For the baseline Fock state, $n_{\mathrm{ref}} = 1$, $G_1 = 0.2\omega_m$ and $G_2 = 0.05\omega_m$, this gives $\Delta_c^{\mathrm{ref}} = -0.19\omega_m$, which coincides with the strong charging resonance found numerically in the supplied simulation. Equation (11) should be viewed as an operating-point prescription rather than an exact dressed cavity eigenfrequency: the full Hamiltonian retains the $b^2 + b^{\dagger 2}$ terms, the linear displacement physics, the atom–cavity coupling and the drive. For the central state-to-state comparison we therefore determine the optimal Δ_c numerically for each initial mechanical state instead of imposing Eq. (11).

We set $\Delta_a = -\omega_m$ throughout, i.e. $\omega_l = \omega_0 + \omega_m$. Because the cavity detuning is generally nonzero, this condition is *not* identical to $\omega_f = \omega_0 + \omega_m$; rather $\omega_f - \omega_0 = \omega_m + \Delta_c$. This distinction matters when the cavity resonance is shifted by the optomechanical interactions.

Charging protocol and figures of merit. The atoms start in their ground state, $|\psi_0\rangle_B = |gg\rangle$, and the optical mode starts empty. The mechanical mode carries the charge and is prepared in a state ρ_m that we vary. The whole system evolves unitarily under Eq. (8), and the battery state is obtained by tracing out the charger,

$$\rho_B(t) = \mathrm{Tr}_C\big[U(t)\,\rho_{\mathrm{tot}}(0)\,U^\dagger(t)\big], \qquad U(t) = e^{-iHt}. \tag{12}$$

The useful stored energy is the ergotropy [4]. Let

$$H_B = \sum_i \varepsilon_i\,|\varepsilon_i\rangle\,\langle\varepsilon_i|\,, \qquad \rho_B = \sum_j r_j\,|r_j\rangle\,\langle r_j|\,, \tag{13}$$

with $\varepsilon_i \le \varepsilon_{i+1}$ and $r_j \ge r_{j+1}$. The associated passive state is $\sigma_{\rho_B} = \sum_i r_i\,|\varepsilon_i\rangle\,\langle\varepsilon_i|$, and

$$\mathcal{E}(t) = \mathrm{Tr}\left[\rho_B(t)H_B\right] - \sum_i r_i\varepsilon_i. \tag{14}$$

Adding a constant to H_B does not change the ergotropy. In the numerics we therefore use the equivalent positive Hamiltonian $H_B^{(+)} = \omega_0 \sum_i \sigma_+^i\sigma_-^i$ and normalize by the two-cell capacity $E_{\mathrm{cap}} = E_{ee} - E_{gg} = 2\omega_0$. Thus $\mathcal{E}_{\max} = \max_t \mathcal{E}(t)/E_{\mathrm{cap}} = 1$ corresponds to a fully excited battery. This is the *local* ergotropy of the reduced atomic state and assumes that the atom–charger couplings can be switched off before the optimal unitary extraction step. Entanglement between the two cells is measured by the Wootters concurrence [104]. For the charger we use two independent diagnostics: the Mandel parameter [99],

$$Q = \frac{\langle n_b^2\rangle - \langle n_b\rangle^2}{\langle n_b\rangle} - 1 = \frac{\mathrm{Var}(n_b)}{\langle n_b\rangle} - 1, \tag{15}$$

which is negative for sub-Poissonian statistics, and the Wigner negativity [101],

$$\delta_W = \int \big|W(\alpha)\big|\,d^2\alpha - 1, \tag{16}$$

which vanishes for every state with a non-negative Wigner function. It is a measure of Wigner non-positivity, not a universal measure of optical non-classicality: an ideal squeezed vacuum has $\delta_W = 0$ despite being non-classical.

The controlled comparison. We prepare the mechanical charger in five states – Fock $|\bar{n}\rangle$, coherent, thermal, squeezed vacuum and even cat $\propto |\alpha\rangle + |-\alpha\rangle$ – all constrained to the same mean occupation $\langle n_b\rangle = \bar{n}$. The squeezing parameter and cat amplitude are fixed by bisection so that the constraint holds to four decimal places. Because the initial mechanical energy above the common zero-point term is $\omega_m\langle n_b\rangle$, matching $\langle n_b\rangle$ matches the *initial mechanical mean energy*. It does not, however, guarantee equal total energy input over the charging interval: the classical cavity drive is continuously present and the work it performs can depend on the evolving state. Accordingly, differences in $\mathcal{E}_{\max}$ demonstrate sensitivity to charger-state structure at fixed initial mechanical energy and fixed drive parameters, but do not by themselves constitute a resource-normalized thermodynamic advantage. Thermal states are mixed, and since ergotropy is non-linear in the state we evolve each Fock component separately and average the resulting *battery* density matrices before evaluating Eq. (14).

One further control is essential. Because the resonance condition (11) depends on n_b, a single shared Δ_c would favour whichever charger happens to sit at it. We therefore optimise Δ_c separately for each charger and quote every state at its own best detuning. This avoids penalizing any charger merely because a single shared operating point happens to favor another state.

For the open-system check we use the Lindblad equation

$$\dot{\rho} = -i[H,\rho] + \kappa\,\mathcal{D}[a]\rho + \gamma(\bar{n}_{\mathrm{th}}+1)\mathcal{D}[b]\rho + \gamma\bar{n}_{\mathrm{th}}\mathcal{D}[b^\dagger]\rho, \tag{17}$$

where $\mathcal{D}[o]\rho = o\rho o^\dagger - \frac{1}{2}\{o^\dagger o, \rho\}$. Atomic spontaneous emission and pure dephasing are not included in this auxiliary robustness test, so the dissipative results should not be read as a complete device-level error budget.

Unless stated otherwise we use $\omega_m = 1$, $G_1 = 0.2\omega_m$, $g = 0.09\omega_m$, $E_l = 0.01\omega_m$ and $G_2 = 0.05\omega_m$. The Hamiltonian is diagonalised once per parameter point and states are propagated spectrally. Convergence was verified by increasing the Fock truncations from $(N_a, N_b) = (14, 8)$ to $(26, 12)$, over which $\mathcal{E}_{\max}$ was stable to five decimal places.

3 Results and numerical discussion

Figure 2 characterizes the five initial mechanical states in phase space. At $\langle n_b \rangle = 1$, the Fock state $|1\rangle$ has the largest Wigner negativity in the set, $\delta_W \simeq 0.426$, and the even cat has $\delta_W \simeq 0.272$. The coherent, thermal and ideal squeezed-vacuum states all have non-negative Wigner functions and therefore $\delta_W = 0$. The squeezed state is nevertheless non-classical through its quadrature noise, illustrating why Wigner negativity must not be identified with non-classicality in general.

Figure 3 shows the same states in the phonon-number basis. Their exact number variances at unit mean are 0 (Fock), 1 (coherent), 1.439 (even cat), 2 (thermal) and 4 (squeezed vacuum), corresponding to $Q = -1, 0, 0.439, 1, 3$, respectively. The distinction between the Fock and coherent states is particularly clean: they have the two narrowest number distributions, while the remaining states are super-Poissonian.

Figure 6 is a representative time-domain comparison at the common reference detuning used in the supplied dynamical data. It is useful for visualizing the different coherent oscillations, but its peak values are *not* the optimized state-by-state numbers quoted below. This distinction resolves the otherwise apparent mismatch between Figs. 6 and 7. The concurrence and ergotropy often rise in the same time windows, but this correlation does not establish that entanglement causes the energy transfer.

The optimized comparison is shown in Fig. 7. With the initial mechanical mean energy fixed and Δ_c optimized separately for each state, the maximum normalized ergotropies are approximately 0.280 (Fock), 0.094 (coherent), 0.033 (squeezed vacuum), 0.032 (even cat), and 0.022 (thermal). The Fock state therefore delivers about three times the coherent value and about thirteen times the thermal value for this parameter set. The comparison establishes that equal initial mean mechanical energy does not fix the charging outcome; it does not by itself prove equal total energetic cost because the classical drive remains active.

Panel (b) of Fig. 7 also shows why Wigner negativity is not a useful predictor here. Three states with $\delta_W = 0$ have substantially different ergotropies, while the Wigner-negative even cat underperforms the coherent state. Number statistics are more informative at the top of the ranking: the Fock and coherent states have the smallest variances and are the two best chargers. However, variance is not a complete ordering variable, because the squeezed vacuum has the largest variance yet slightly exceeds the cat and thermal values. We therefore use number statistics as a mechanism-guided diagnostic rather than as a universal charging monotone.

Figure 8 probes that mechanism by varying G_2. The Fock-to-coherent ratio grows from 1.33 at $G_2 = 0$ through 2.31, 3.04 and 4.48 to 5.17 at $G_2 = 0.08\omega_m$. This is consistent with the idea that the number-dependent quadratic shift makes broad number distributions sample a broader set of effective detunings. Importantly, the ratio is already above unity at $G_2 = 0$; the quadratic interaction therefore *amplifies* the state dependence rather than generating it entirely. Because the full quadratic term also contains $b^2 + b^{\dagger 2}$, this dephasing picture should be understood as a physically motivated interpretation rather than an exact reduction of the dynamics.

Figure 4 maps the Fock/coherent ratio over the (g, E_l) plane using the common reference-detuning prescription of Eq. (11). The Fock state leads over much of the plotted region, while the ratio drops below unity in parts of the weak-drive and strong-coupling edges. The map therefore

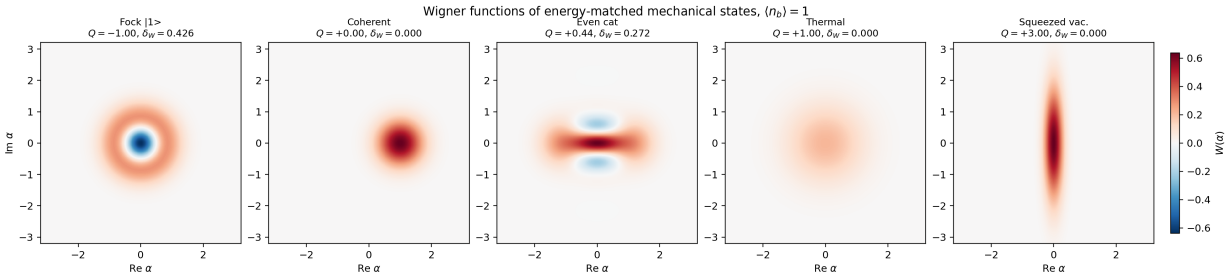


Figure 2: Wigner functions of the five mechanical states at the same initial mean occupation $\langle n_b \rangle = 1$. The values of Q and δ_W are evaluated from the ideal input states rather than from a truncated phase-space grid. The coherent, thermal and squeezed-vacuum states have non-negative Wigner functions even though the squeezed vacuum is non-classical.

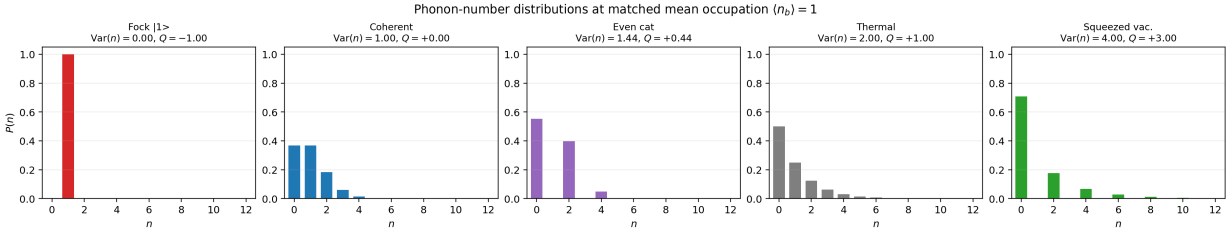


Figure 3: Phonon-number distributions of the five energy-matched mechanical states. At $\langle n_b \rangle = 1$ the exact variances are 0, 1, 1.439, 2 and 4 for Fock, coherent, even-cat, thermal and squeezed-vacuum states, respectively.

shows that the advantage is operating-point dependent. Because Δ_c is not re-optimized at every grid point, the contour boundaries should be interpreted as a guide to parameter selection rather than as a universal phase boundary.

Figure 5 gives an auxiliary open-system test using Eq. (17). Within that reduced-truncation calculation, modest cavity and mechanical damping preserve the ordering and change the Fock-to-coherent ratio from 5.01 to 4.64, whereas adding a mechanical bath with $\bar{n}_{\mathrm{th}} = 1$ strongly suppresses the Fock result. The absolute maxima in this panel should not be compared directly with the optimized values of Fig. 7, because the dissipative run uses a coarser Hilbert-space truncation and a different detuning protocol. The robust conclusion is qualitative: number-selective charging is sensitive to thermal broadening of the mechanical state. A realistic device study must additionally include atomic relaxation/dephasing and experimentally attainable coupling strengths.

Figure 9 checks the optimized comparison at a larger matched mean occupation. The supplied data show that the Fock/coherent and Fock/thermal ratios increase on going from $\langle n_b \rangle = 1$ to 3. As at unit mean, this should be interpreted as a state-dependent charging result at matched initial mechanical energy, not as a complete resource-normalized efficiency comparison. The result is also a reminder that a shared detuning can create spurious inversions when the optimal resonances of different states separate.

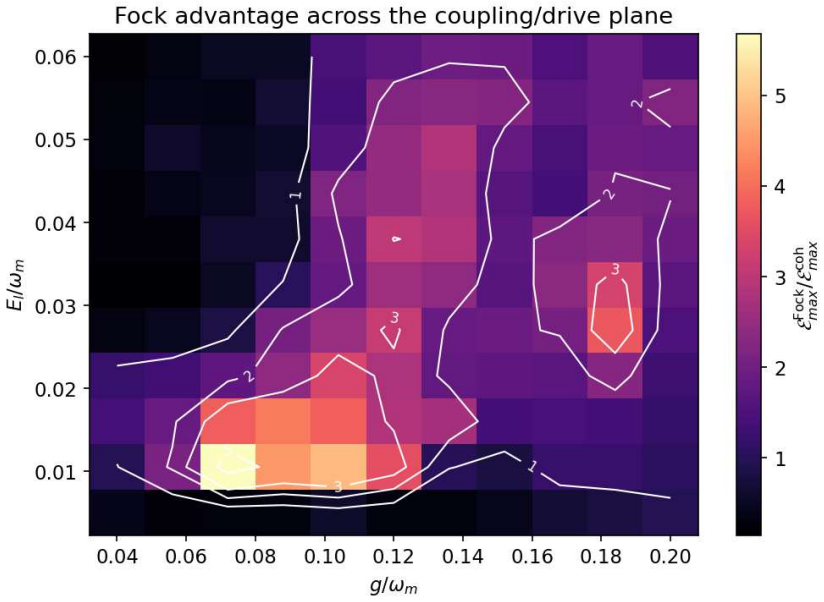


Figure 4: Fock/coherent ergotropy ratio across the (g, E_l) plane at fixed $G_1 = 0.2\omega_m$ and $G_2 = 0.05\omega_m$, using the reference detuning of Eq. (11). White contours mark ratios of 1, 2, 3 and 5. Because the detuning is not re-optimized at every grid point, this map is an operating-point guide rather than a universal boundary.

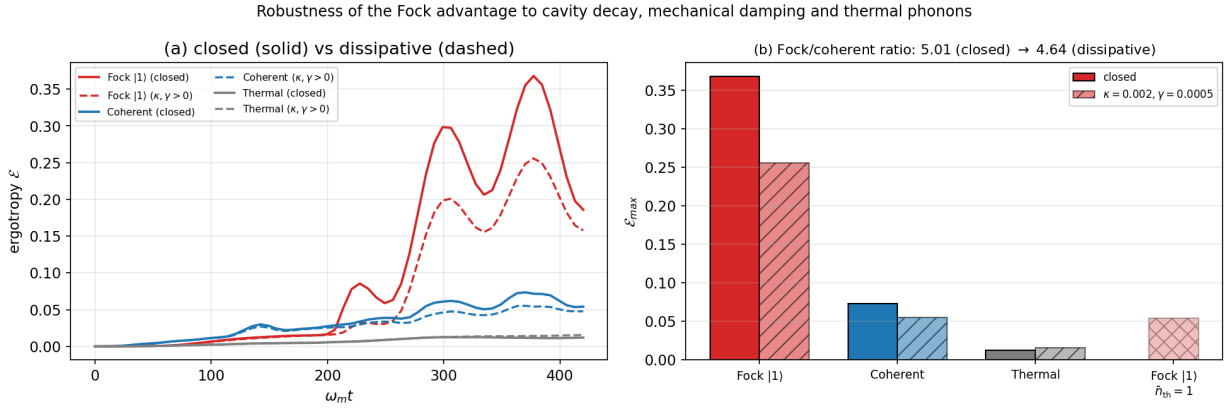


Figure 5: Open-system robustness test from Eq. (17). (a) Ergotropy versus time for the three states in the closed calculation (solid) and with $\kappa = 0.002\omega_m$, $\gamma = 0.0005\omega_m$ (dashed). (b) Maxima, including a mechanical bath with $\bar{n}_{\rm th} = 1$. These data were obtained with the reduced truncation used for the Lindblad calculation and should be compared within the panel, not directly with the optimized maxima of Fig. 7.

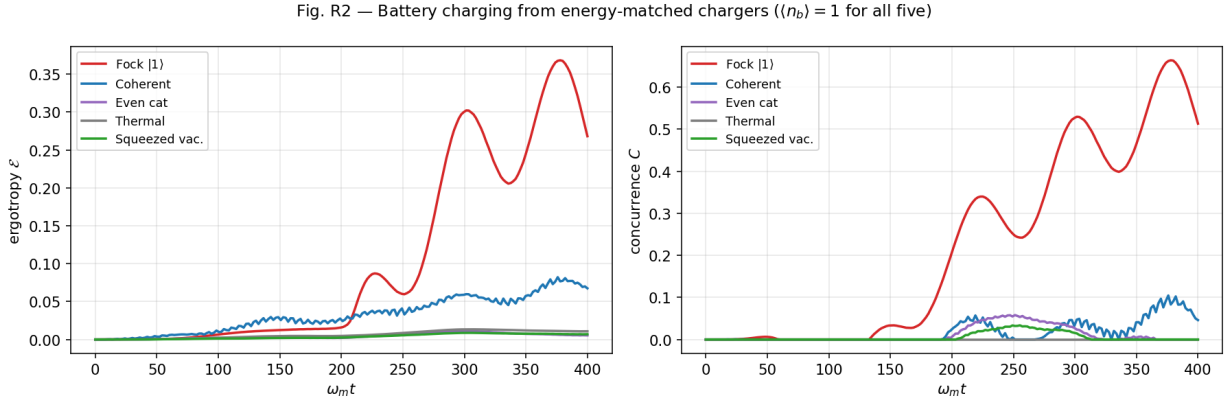


Figure 6: Representative time evolution of the battery ergotropy (left) and two-cell concurrence (right) for the energy-matched mechanical states at the common reference detuning used in the supplied dynamical data. The separate optimized-detuning comparison is given in Fig. 7.

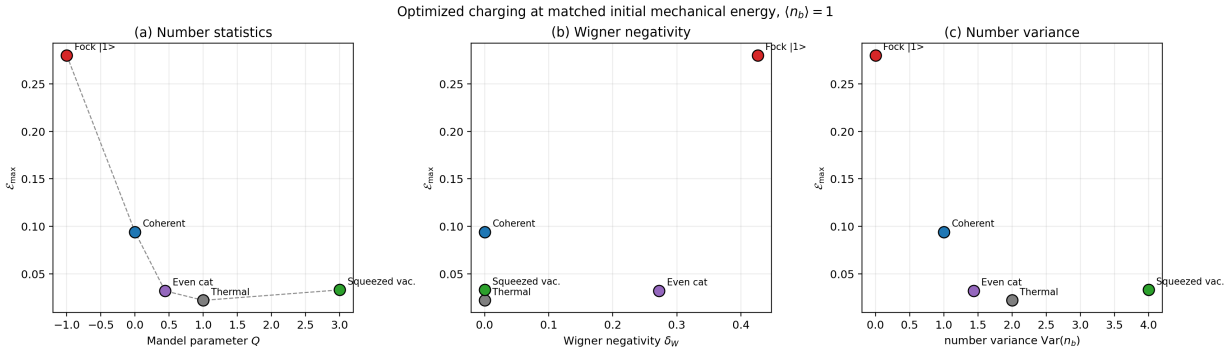


Figure 7: Maximum ergotropy at matched initial mechanical energy with the cavity detuning optimized separately for each state. (a) Mandel parameter, (b) Wigner negativity, and (c) number variance. Wigner negativity does not order the performance; low number variance distinguishes the two best chargers but is not an exact monotone across all five states.

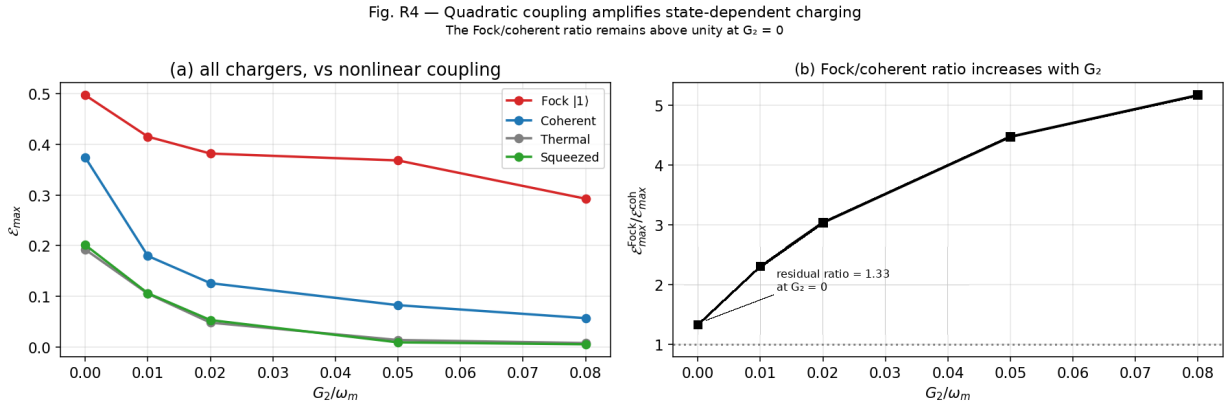


Figure 8: Dependence on the quadratic optomechanical coupling. (a) Maximum ergotropy for the plotted states and (b) Fock/coherent ratio. The ratio rises from 1.33 at $G_2 = 0$ to 5.17 at $G_2 = 0.08\omega_m$, showing that the quadratic term strongly amplifies an advantage that is already nonzero at $G_2 = 0$.

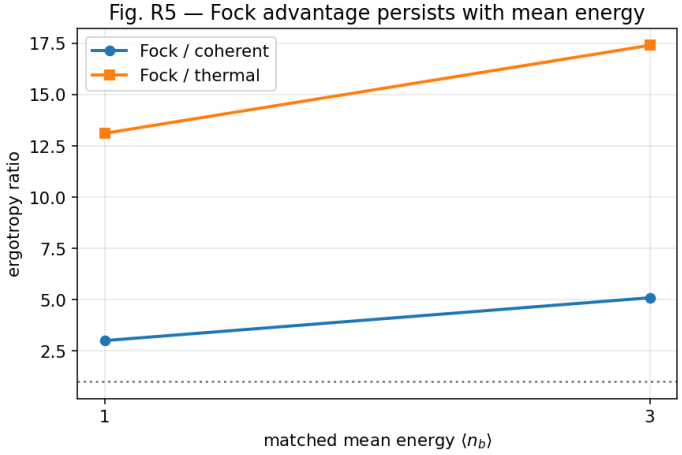


Figure 9: Robustness with respect to the matched initial mean mechanical occupation. In the supplied optimized-detuning data, the Fock/coherent and Fock/thermal ergotropy ratios increase between $\langle n_b \rangle = 1$ and 3.

4 Conclusion

We have compared five mechanically prepared charger states in a driven atom–optomechanical quantum-battery model while fixing their initial mean mechanical occupation and, for the headline comparison, optimizing the cavity detuning separately for each state. These two controls remove two common confounders: trivial changes of initial mean mechanical energy and accidental off-resonant operation.

For the parameter set studied here, the number-definite Fock state gives the largest local battery ergotropy, followed by the coherent state, while the thermal, even-cat and squeezed-vacuum states remain much lower. Wigner negativity does not reproduce this ordering. In particular, the ideal squeezed vacuum has a non-negative Wigner function, the coherent and thermal states are also Wigner-positive, and the Wigner-negative cat still performs below the coherent state. Low number variance provides a more useful physical clue: the Fock and coherent states are the two narrowest number distributions and the two best chargers. The three broader states are not strictly ordered by variance, so neither the Mandel parameter nor the variance should be promoted to a universal charging monotone.

The G_2 scan supports a number-dependent resonance interpretation. Increasing quadratic coupling greatly increases the Fock/coherent ratio, consistent with broad number distributions sampling different effective detunings. The advantage does not vanish at $G_2 = 0$, however, and the full quadratic Hamiltonian also contains two-phonon terms. The most defensible conclusion is therefore that quadratic coupling strongly *amplifies* state-dependent charging in this regime, not that it is the sole origin of the effect.

The open-system calculation leads to a similarly qualified result. In the chosen reduced-truncation example, modest cavity and mechanical damping preserve the ranking, while a thermal mechanical bath strongly suppresses the number-definite advantage. This points to thermal state preparation as an important experimental consideration, but it does not establish that quality factors or other decoherence channels are unimportant. Atomic relaxation and pure dephasing were not included, and the assumed single-photon nonlinear couplings are substantially stronger than those available in many present membrane-in-the-middle implementations.

Finally, equal initial mechanical energy is not the same as equal total charging cost in a continuously driven system. The classical drive can perform a state-dependent amount of work, which has not been integrated explicitly in the present data. A fully resource-normalized follow-up should therefore report the work supplied by the drive, the mechanical energy change, and the battery energy/ergotropy on the same footing. Within that limitation, the present results demonstrate a clear and reproducible sensitivity of optomechanical battery charging to the quantum state's number statistics and to the number-dependent resonance structure of the device.

Declarations

Author contributions. Both authors contributed to the conception and development of the study, analysis and interpretation of the results, and preparation and revision of the manuscript. Both authors read and approved the final manuscript.

Funding. The authors declare that no specific funding was received for this work.

Data availability. No separate data are available for this study. No external datasets were used; all numerical results needed to support the conclusions are presented in the manuscript and its figures.

Code availability. No public code repository is associated with this study.

Competing interests. The authors declare that they have no competing interests.

Ethics approval. Not applicable. This study did not involve human participants, human data, animals, or biological material.

Consent to participate. Not applicable.

Consent for publication. Not applicable.

Acknowledgements. The authors have no acknowledgements to declare.

References

[1] S. Vinjanampathy and J. Anders, *Quantum thermodynamics*, Contemp. Phys. **57**, 545 (2016).

[2] J. Goold, M. Huber, A. Riera, L. del Rio, and P. Skrzypczyk, *The role of quantum information in thermodynamics—a topical review*, J. Phys. A **49**, 143001 (2016).

[3] R. Kosloff, *Quantum thermodynamics: A dynamical viewpoint*, Entropy **15**, 2100 (2013).

[4] A. E. Allahverdyan, R. Balian, and T. M. Nieuwenhuizen, *Maximal work extraction from finite quantum systems*, Europhys. Lett. **67**, 565 (2004).

[5] W. Pusz and S. L. Woronowicz, *Passive states and KMS states for general quantum systems*, Commun. Math. Phys. **58**, 273 (1978).

[6] A. Lenard, *Thermodynamical proof of the Gibbs formula for elementary quantum systems*, J. Stat. Phys. **19**, 575 (1978).

[7] R. Alicki and M. Fannes, *Entanglement boost for extractable work from ensembles of quantum batteries*, Phys. Rev. E **87**, 042123 (2013).

[8] F. C. Binder, S. Vinjanampathy, K. Modi, and J. Goold, *Quantacell: powerful charging of quantum batteries*, New J. Phys. **17**, 075015 (2015).

[9] F. Campaioli, F. A. Pollock, and S. Vinjanampathy, *Quantum batteries*, in *Thermodynamics in the Quantum Regime* (Springer, 2018), p. 207.

[10] F. Campaioli, S. Gherardini, J. Q. Quach, M. Polini, and G. M. Andolina, *Colloquium: Quantum batteries*, Rev. Mod. Phys. **96**, 031001 (2024).

[11] A. Shokri, E. Faizi, and M. B. Arjmandi, *Entanglement-assisted charging of quantum batteries within optomechanical framework*, Phys. Rev. E **111**, 064117 (2025).

[12] F. Campaioli, F. A. Pollock, F. C. Binder, L. Céleri, J. Goold, S. Vinjanampathy, and K. Modi, *Enhancing the charging power of quantum batteries*, Phys. Rev. Lett. **118**, 150601 (2017).

[13] D. Ferraro, M. Campisi, G. M. Andolina, V. Pellegrini, and M. Polini, *High-power collective charging of a solid-state quantum battery*, Phys. Rev. Lett. **120**, 117702 (2018).

[14] G. M. Andolina, M. Keck, A. Mari, M. Campisi, V. Giovannetti, and M. Polini, *Extractable work, the role of correlations, and asymptotic freedom in quantum batteries*, Phys. Rev. Lett. **122**, 047702 (2019).

[15] G. M. Andolina, M. Keck, A. Mari, V. Giovannetti, and M. Polini, *Quantum versus classical many-body batteries*, Phys. Rev. B **99**, 205437 (2019).

[16] D. Rossini, G. M. Andolina, D. Rosa, M. Carrega, and M. Polini, *Quantum advantage in the charging process of Sachdev-Ye-Kitaev batteries*, Phys. Rev. Lett. **125**, 236402 (2020).

[17] J.-Y. Gyhm, D. Šafránek, and D. Rosa, *Quantum charging advantage cannot be extensive without global operations*, Phys. Rev. Lett. **128**, 140501 (2022).

[18] S. Julià-Farré, T. Salamon, A. Riera, M. N. Bera, and M. Lewenstein, *Bounds on the capacity and power of quantum batteries*, Phys. Rev. Research **2**, 023113 (2020).

[19] T. P. Le, J. Levinsen, K. Modi, M. M. Parish, and F. A. Pollock, *Spin-chain model of a many-body quantum battery*, Phys. Rev. A **97**, 022106 (2018).

[20] Y. Yao and X. Q. Shao, *Optimal charging of open spin-chain quantum batteries via homodyne-based feedback control*, Phys. Rev. E **106**, 014138 (2022).

[21] D. Rossini, G. M. Andolina, and M. Polini, *Many-body localized quantum batteries*, Phys. Rev. B **100**, 115142 (2019).

[22] S. Ghosh, T. Chanda, and A. Sen(De), *Enhancement in the performance of a quantum battery by ordered and disordered interactions*, Phys. Rev. A **101**, 032115 (2020).

[23] M. B. Arjmandi, H. Mohammadi, A. Saguia, M. S. Sarandy, and A. C. Santos, *Localization effects in disordered quantum batteries*, Phys. Rev. E **108**, 064106 (2023).

[24] M. B. Arjmandi, H. Mohammadi, and A. C. Santos, *Enhancing self-discharging process with disordered quantum batteries*, Phys. Rev. E **105**, 054115 (2022).

[25] A. Crescente, M. Carrega, M. Sassetti, and D. Ferraro, *Ultrafast charging in a two-photon Dicke quantum battery*, Phys. Rev. B **102**, 245407 (2020).

[26] D. L. Yang, F. M. Yang, and F. Q. Dou, *Three-level Dicke quantum battery*, Phys. Rev. B **109**, 235432 (2024).

[27] W. Zhang, S. Wang, C. Wu, and G. Wang, *Quantum battery based on dipole-dipole interaction and external driving field*, Phys. Rev. E **107**, 054125 (2023).

[28] C. K. Hu, J. Qiu, P. J. P. Souza, J. Yuan, Y. Zhou, L. Zhang, *et al.*, *Optimal charging of a superconducting quantum battery*, Quantum Sci. Technol. **7**, 045018 (2022).

[29] F. Q. Dou and F. M. Yang, *Superconducting transmon qubit-resonator quantum battery*, Phys. Rev. A **107**, 023725 (2023).

[30] F. Q. Dou, Y. J. Wang, and J. A. Sun, *Highly efficient charging and discharging of three-level quantum batteries through shortcuts to adiabaticity*, Front. Phys. **17**, 31503 (2022).

[31] J. Q. Quach, K. E. McGhee, L. Ganzer, D. M. Rouse, B. W. Lovett, E. M. Gauger, *et al.*, *Superabsorption in an organic microcavity: Toward a quantum battery*, Sci. Adv. **8**, eabk3160 (2022).

[32] J. Joshi and T. S. Mahesh, *Experimental investigation of a quantum battery using star-topology NMR spin systems*, Phys. Rev. A **106**, 042601 (2022).

[33] J. Roßnagel, S. T. Dawkins, K. N. Tolazzi, O. Abah, E. Lutz, F. Schmidt-Kaler, and K. Singer, *A single-atom heat engine*, Science **352**, 325 (2016).

[34] G. Maslennikov, S. Ding, R. Hablützel, J. Gan, A. Roulet, S. Nimmrichter, *et al.*, *Quantum absorption refrigerator with trapped ions*, Nat. Commun. **10**, 202 (2019).

[35] D. von Lindenfels, O. Gräb, C. T. Schmiegelow, V. Kaushal, J. Schulz, M. T. Mitchison, *et al.*, *Spin heat engine coupled to a harmonic-oscillator flywheel*, Phys. Rev. Lett. **123**, 080602 (2019).

[36] J. Klatzow, J. N. Becker, P. M. Ledingham, C. Weinzetl, K. T. Kaczmarek, D. J. Saunders, *et al.*, *Experimental demonstration of quantum effects in the operation of microscopic heat engines*, Phys. Rev. Lett. **122**, 110601 (2019).

[37] A. C. Santos, *Quantum advantage of two-level batteries in the self-discharging process*, Phys. Rev. E **103**, 042118 (2021).

[38] A. C. Santos, A. Saguia, and M. S. Sarandy, *Stable and charge-switchable quantum batteries*, Phys. Rev. E **101**, 062114 (2020).

[39] J. Q. Quach and W. J. Munro, *Using dark states to charge and stabilize open quantum batteries*, Phys. Rev. Applied **14**, 024092 (2020).

[40] J. Liu, D. Segal, and G. Hanna, *Loss-free excitonic quantum battery*, J. Phys. Chem. C **123**, 18303 (2019).

[41] F. H. Kamin, F. T. Tabesh, S. Salimi, F. Kheirandish, and A. C. Santos, *Non-Markovian effects on charging and self-discharging process of quantum batteries*, New J. Phys. **22**, 083007 (2020).

[42] D. Morrone, M. A. C. Rossi, A. Smirne, and M. G. Genoni, *Charging a quantum battery in a non-Markovian environment: a collisional model approach*, Quantum Sci. Technol. **8**, 035007 (2023).

[43] F. H. Kamin, F. T. Tabesh, S. Salimi, and A. C. Santos, *Entanglement, coherence, and charging process of quantum batteries*, Phys. Rev. E **102**, 052109 (2020).

[44] K. Araya-Sossa and D. Mundarain, *Geometrical correlations as a resource for nonlocal extractable work*, Ann. Phys. **404**, 81 (2019).

[45] M. B. Arjmandi, A. Shokri, E. Faizi, and H. Mohammadi, *Performance of quantum batteries with correlated and uncorrelated chargers*, Phys. Rev. A **106**, 062609 (2022).

[46] M. Aspelmeyer, T. J. Kippenberg, and F. Marquardt, *Cavity optomechanics*, Rev. Mod. Phys. **86**, 1391 (2014).

[47] W. P. Bowen and G. J. Milburn, *Quantum Optomechanics* (CRC Press, Boca Raton, 2015).

[48] P. Meystre, *A short walk through quantum optomechanics*, Ann. Phys. (Berlin) **525**, 215 (2013).

[49] D. Hu, S. Y. Huang, J. Q. Liao, L. Tian, and H. S. Goan, *Quantum coherence in ultrastrong optomechanics*, Phys. Rev. A **91**, 013812 (2015).

[50] M. J. Weaver, F. Buters, F. Luna, H. Eerkens, K. Heeck, S. de Man, and D. Bouwmeester, *Coherent optomechanical state transfer between disparate mechanical resonators*, Nat. Commun. **8**, 824 (2017).

[51] B. B. Li, L. Ou, Y. Lei, and Y. C. Liu, *Cavity optomechanical sensing*, Nanophotonics **10**, 2799 (2021).

[52] M. Toroš and T. S. Monteiro, *Quantum sensing and cooling in three-dimensional levitated cavity optomechanics*, Phys. Rev. Research **2**, 023228 (2020).

[53] Y. Xia, A. R. Agrawal, C. M. Pluchar, A. J. Brady, Z. Liu, Q. Zhuang, and Z. Zhang, *Entanglement-enhanced optomechanical sensing*, Nat. Photonics **17**, 470 (2023).

[54] S. Qvarfort, A. D. K. Plato, D. E. Bruschi, F. Schneiter, D. Braun, A. Serafini, and D. Rätzel, *Optimal estimation of time-dependent gravitational fields with quantum optomechanical systems*, Phys. Rev. Research **3**, 013159 (2021).

[55] S. Barzanjeh, A. Xuereb, S. Gröblacher, M. Paternostro, C. A. Regal, and E. M. Weig, *Optomechanics for quantum technologies*, Nat. Phys. **18**, 15 (2022).

[56] S. L. Danilishin, F. Y. Khalili, and H. Miao, *Advanced quantum techniques for future gravitational-wave detectors*, Living Rev. Relativ. **22**, 2 (2019).

[57] N. Didier, S. Pugnetti, Y. M. Blanter, and R. Fazio, *Quantum transducer in circuit optomechanics*, Solid State Commun. **198**, 61 (2014).

[58] S. Deléglise, T. Capelle, X. Chen, T. Jacqmin, R. Braive, I. Robert-Philip, and A. Heidmann, *Hybrid optomechanical systems as transducers for quantum information*, in *Quantum Information and Measurement* (Optica Publishing Group, 2017), paper QF3C.3.

[59] K. Stannigel, P. Komar, S. J. M. Habraken, S. D. Bennett, M. D. Lukin, P. Zoller, and P. Rabl, *Optomechanical quantum information processing with photons and phonons*, Phys. Rev. Lett. **109**, 013603 (2012).

[60] B. Rogers, N. Lo Gullo, G. De Chiara, G. M. Palma, and M. Paternostro, *Hybrid optomechanics for quantum technologies*, Quantum Meas. Quantum Metrol. **2**, 11 (2014).

[61] Y. J. Xu, S. S. Wang, M. R. Chen, and Q. H. Liao, *Entanglement and statistical properties in cavity optomechanics with a single atom*, Laser Phys. **29**, 065202 (2021).

[62] M. F. Alotaibi, E. M. Khalil, and M. Y. Abd-Rabbou, *Dynamics of an atomic system associated with a cavity-optomechanical system*, Results Phys. **37**, 105540 (2022).

[63] F. Eftekhari, M. K. Tavassoly, A. Behjat, and M. J. Faghihi, *Entanglement and atomic inversion in a dissipative two-atom-optomechanical system*, Opt. Laser Technol. **168**, 109934 (2024).

[64] S. K. Singh, J. X. Peng, M. Asjad, and M. Mazaheri, *Entanglement and coherence in a hybrid Laguerre–Gaussian rotating cavity optomechanical system with two-level atoms*, J. Phys. B **54**, 215502 (2021).

[65] J. D. Teufel, T. Donner, D. Li, J. W. Harlow, M. S. Allman, K. Cicak, *et al.*, *Sideband cooling of micromechanical motion to the quantum ground state*, Nature **475**, 359 (2011).

[66] J. Chan, T. P. M. Alegre, A. H. Safavi-Naeini, J. T. Hill, A. Krause, S. Gröblacher, *et al.*, *Laser cooling of a nanomechanical oscillator into its quantum ground state*, Nature **478**, 89 (2011).

[67] A. D. O'Connell, M. Hofheinz, M. Ansmann, R. C. Bialczak, M. Lenander, E. Lucero, *et al.*, *Quantum ground state and single-phonon control of a mechanical resonator*, Nature **464**, 697 (2010).

[68] U. Delić, M. Reisenbauer, K. Dare, D. Grass, V. Vuletić, N. Kiesel, and M. Aspelmeyer, *Cooling of a levitated nanoparticle to the motional quantum ground state*, Science **367**, 892 (2020).

[69] L. Magrini, P. Rosenzweig, C. Bach, A. Deutschmann-Olek, S. G. Hofer, S. Hong, *et al.*, *Real-time optimal quantum control of mechanical motion at room temperature*, Nature **595**, 373 (2021).

[70] M. Rossi, D. Mason, J. Chen, Y. Tsaturyan, and A. Schliesser, *Measurement-based quantum control of mechanical motion*, Nature **563**, 53 (2018).

[71] S. Hong, R. Riedinger, I. Marinković, A. Wallucks, S. G. Hofer, R. A. Norte, *et al.*, *Hanbury Brown and Twiss interferometry of single phonons from an optomechanical resonator*, Science **358**, 203 (2017).

[72] R. Riedinger, S. Hong, R. A. Norte, J. A. Slater, J. Shang, A. G. Krause, *et al.*, *Non-classical correlations between single photons and phonons from a mechanical oscillator*, Nature **530**, 313 (2016).

[73] Y. Chu, P. Kharel, T. Yoon, L. Frunzio, P. T. Rakich, and R. J. Schoelkopf, *Creation and control of multi-phonon Fock states in a bulk acoustic-wave resonator*, Nature **563**, 666 (2018).

[74] K. J. Satzinger, Y. P. Zhong, H.-S. Chang, G. A. Peairs, A. Bienfait, M.-H. Chou, *et al.*, *Quantum control of surface acoustic-wave phonons*, Nature **563**, 661 (2018).

[75] P. Arrangoiz-Arriola, E. A. Wollack, Z. Wang, M. Pechal, W. Jiang, T. P. McKenna, *et al.*, *Resolving the energy levels of a nanomechanical oscillator*, Nature **571**, 537 (2019).

[76] E. E. Wollman, C. U. Lei, A. J. Weinstein, J. Suh, A. Kronwald, F. Marquardt, *et al.*, *Quantum squeezing of motion in a mechanical resonator*, Science **349**, 952 (2015).

[77] J.-M. Pirkkalainen, E. Damskägg, M. Brandt, F. Massel, and M. A. Sillanpää, *Squeezing of quantum noise of motion in a micromechanical resonator*, Phys. Rev. Lett. **115**, 243601 (2015).

[78] F. Lecocq, J. B. Clark, R. W. Simmonds, J. Aumentado, and J. D. Teufel, *Quantum non-demolition measurement of a nonclassical state of a massive object*, Phys. Rev. X **5**, 041037 (2015).

[79] T. A. Palomaki, J. D. Teufel, R. W. Simmonds, and K. W. Lehnert, *Entangling mechanical motion with microwave fields*, Science **342**, 710 (2013).

[80] I. Marinković, A. Wallucks, R. Riedinger, S. Hong, M. Aspelmeyer, and S. Gröblacher, *Optomechanical Bell test*, Phys. Rev. Lett. **121**, 220404 (2018).

[81] M. Bild, M. Fadel, Y. Yang, U. von Lüpke, P. Martin, A. Bruno, and Y. Chu, *Schrödinger cat states of a 16-microgram mechanical oscillator*, Science **380**, 274 (2023).

[82] J. D. Thompson, B. M. Zwickl, A. M. Jayich, F. Marquardt, S. M. Girvin, and J. G. E. Harris, *Strong dispersive coupling of a high-finesse cavity to a micromechanical membrane*, Nature **452**, 72 (2008).

[83] J. C. Sankey, C. Yang, B. M. Zwickl, A. M. Jayich, and J. G. E. Harris, *Strong and tunable nonlinear optomechanical coupling in a low-loss system*, Nat. Phys. **6**, 707 (2010).

[84] A. M. Jayich, J. C. Sankey, B. M. Zwickl, C. Yang, J. D. Thompson, S. M. Girvin, *et al.*, *Dispersive optomechanics: a membrane inside a cavity*, New J. Phys. **10**, 095008 (2008).

[85] A. Nunnenkamp, K. Børkje, J. G. E. Harris, and S. M. Girvin, *Cooling and squeezing via quadratic optomechanical coupling*, Phys. Rev. A **82**, 021806(R) (2010).

[86] C. Doolin, B. D. Hauer, P. H. Kim, A. J. R. MacDonald, H. Ramp, and J. P. Davis, *Nonlinear optomechanics in the stationary regime*, Phys. Rev. A **89**, 053838 (2014).

[87] H. Xie, X. Shang, C. G. Liao, Z. H. Chen, and X. M. Lin, *Macroscopic superposition states of a mechanical oscillator in an optomechanical system with quadratic coupling*, Phys. Rev. A **100**, 033803 (2019).

[88] J.-Q. Liao and F. Nori, *Single-photon quadratic optomechanics*, Sci. Rep. **4**, 6302 (2014).

[89] R. J. Glauber, *Coherent and incoherent states of the radiation field*, Phys. Rev. **131**, 2766 (1963).

[90] E. C. G. Sudarshan, *Equivalence of semiclassical and quantum mechanical descriptions of statistical light beams*, Phys. Rev. Lett. **10**, 277 (1963).

[91] A. Mari and J. Eisert, *Positive Wigner functions render classical simulation of quantum computation efficient*, Phys. Rev. Lett. **109**, 230503 (2012).

[92] V. Veitch, C. Ferrie, D. Gross, and J. Emerson, *Negative quasi-probability as a resource for quantum computation*, New J. Phys. **14**, 113011 (2012).

[93] F. Albarelli, M. G. Genoni, L. Lami, and A. Serafini, *Resource theory of quantum non-Gaussianity and Wigner negativity*, Phys. Rev. A **98**, 052350 (2018).

[94] R. Takagi and Q. Zhuang, *Convex resource theory of non-Gaussianity*, Phys. Rev. A **97**, 062337 (2018).

[95] M. Hillery, *Nonclassical distance in quantum optics*, Phys. Rev. A **35**, 725 (1987).

[96] W. Vogel, *Nonclassical states: An observable criterion*, Phys. Rev. Lett. **84**, 1849 (2000).

[97] T. Richter and W. Vogel, *Nonclassicality of quantum states: A hierarchy of observable conditions*, Phys. Rev. Lett. **89**, 283601 (2002).

[98] J. K. Asbóth, J. Calsamiglia, and H. Ritsch, *Computable measure of nonclassicality for light*, Phys. Rev. Lett. **94**, 173602 (2005).

[99] L. Mandel, *Sub-Poissonian photon statistics in resonance fluorescence*, Opt. Lett. **4**, 205 (1979).

[100] C. Weedbrook, S. Pirandola, R. García-Patrón, N. J. Cerf, T. C. Ralph, J. H. Shapiro, and S. Lloyd, *Gaussian quantum information*, Rev. Mod. Phys. **84**, 621 (2012).

[101] A. Kenfack and K. Życzkowski, *Negativity of the Wigner function as an indicator of non-classicality*, J. Opt. B **6**, 396 (2004).

[102] D. F. V. James and J. Jerke, *Effective Hamiltonian theory and its applications in quantum information*, Can. J. Phys. **85**, 625 (2007).

[103] O. Gamel and D. F. V. James, *Time-averaged quantum dynamics and the validity of the effective Hamiltonian model*, Phys. Rev. A **82**, 052106 (2010).

[104] W. K. Wootters, *Entanglement of formation of an arbitrary state of two qubits*, Phys. Rev. Lett. **80**, 2245 (1998).